Four-channel ZnS scintillator measurements of escaping tritons in TFTR

S. J. Zweben

Princeton University, Plasma Physics Laboratory, Princeton, New Jersey 08543

(Received 22 August 1988; accepted for publication 6 December 1988)

A four-channel scintillation detector capable of measuring tritons, protons, and alphas escaping from a tokamak plasma was operated during the 1986 run period of the Tokamak Fusion Test Reactor (TFTR). Signals consistent with the expected 1-MeV triton behavior have been observed during deuterium operation. Backgrounds associated with neutrons/gammas and soft x rays have been evaluated *in situ* and are shown to be at the $\approx 10\%$–20% level for the present detector. Such a detector is capable of measuring escaping alphas in deuterium-tritium-fueled tokamaks such as TFTR.

INTRODUCTION

In past experiments on TFTR and other tokamaks,[1–5] escaping charged fusion products (1-MeV tritons, 3-MeV protons, and 15-MeV protons) have been detected using silicon surface barrier (SSB) detectors. These detectors worked successfully in D/D-fueled plasmas, but it was clear that neutron damage would make the SSB detector unusable in the Tokamak Fusion Test Reactor (TFTR) D/T plasma environment, where the neutron fluence is expected to be $\approx 10^{15}$–10^{16} neutrons/cm^2 over the lifetime of the machine. The SSB detector damage threshold is $\approx 10^{12}$ n/cm^2.[6]

Proposals for replacing the rather delicate single-crystal SSB with the more radiation-resistant multicrystalline ZnS have been made in the past.[7–9] This paper describes the operation of the first such ZnS detector for charged fusion products in a tokamak.

This detector was used during the 1986 TFTR run to measure the flux of escaping 1-MeV tritons onto a ZnS(Ag) scintillator screen located inside the TFTR vacuum vessel but outside the plasma boundary. Particular attention is given to demonstrating that the signals observed in deuterium plasmas are predominantly due to 1-MeV tritons, as expected, and that the observed background effects can be understood as being due to neutrons, gammas, and soft x rays.

Note that in this paper I will refer to 1-MeV triton detection and not to 3.5-MeV alpha detection. However, since the gyroradii (in the plasma) and the ranges (in the scintillator and foils) of these two particles are nearly the same, the detector functions similarly for both particles.

The basic design of the detector is described in Sec. I. The expected triton behavior is discussed in Sec. II. The signal detection methods and calibration are described in Sec. III. The basic demonstration of triton detection is shown through a particular example in Sec. IV. More complete results including explicit background corrections are in Sec. V. Some further measurements of tritons and of 3.7-MeV alphas are described in Sec. VI. A summary of the present status of this detector is in Sec. VII.

I. DETECTOR DESIGN

The general experimental arrangement is shown in Fig. 1. The scintillator detector is mounted on a probe which was inserted into the TFTR vacuum vessel through a valve on the bottom of the machine. For this experiment the detector is positioned well outside the plasma boundary in order to avoid damage from the plasma heat flux. At this position it can detect only those escaping triton orbits which move nearly vertically down toward the probe from above, as shown in the figure and as discussed below. Signals from the probe are carried by optical fibers past a concrete neutron/gamma shield into the basement.

The mechanical design of the detector is shown in Fig. 2

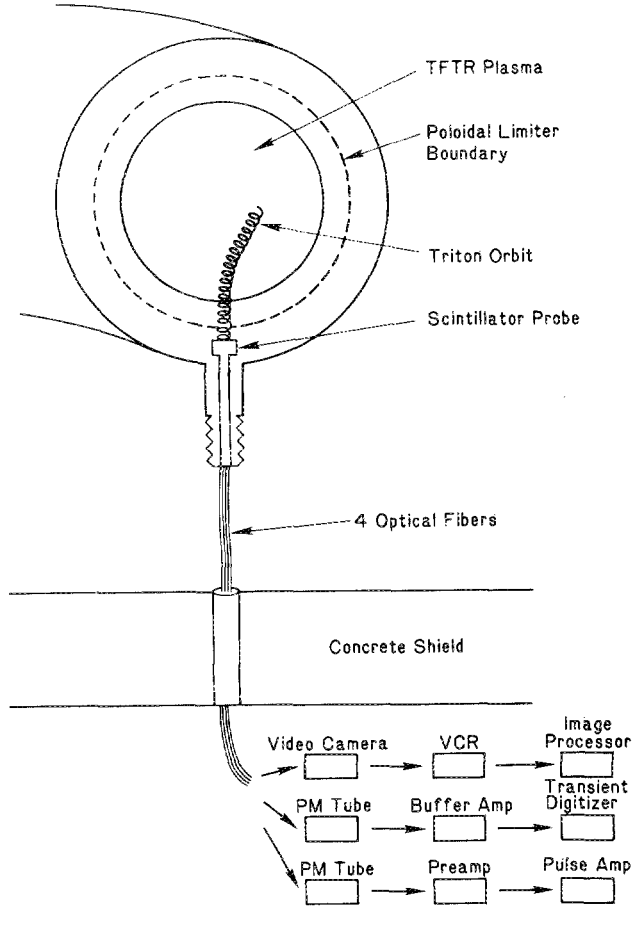

FIG. 1. Overview of the four-channel triton detector as installed on TFTR. The signals were carried by four optical fibers to the shielded basement. Both pulse and flux detection modes were tried.

 0034-6748/89/040576-12$01.30

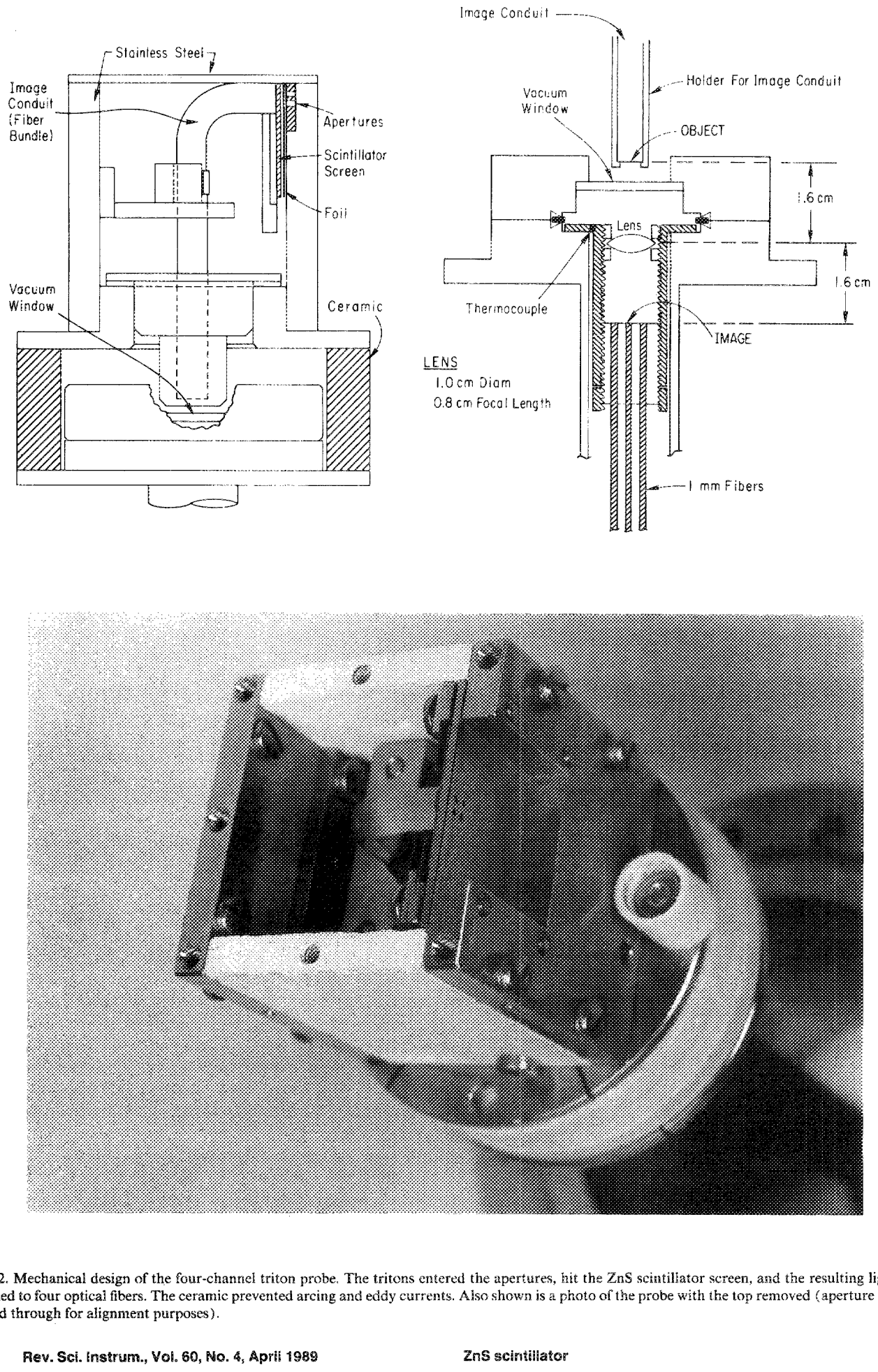

FIG. 2. Mechanical design of the four-channel triton probe. The tritons entered the apertures, hit the ZnS scintillator screen, and the resulting light was coupled to four optical fibers. The ceramic prevented arcing and eddy currents. Also shown is a photo of the probe with the top removed (aperture No. 4 is drilled through for alignment purposes).

and has been described in some detail previously.[10] The scintillator consisted of a substrate of 1 in. × 1 in., 0.15-mm-thick glass onto which was coated an ≈10–15-μm-thick layer of ZnS(Ag), i.e., the standard P11 blue phosphor (see Appendix A for properties of the phosphor). This scintillator was mounted just behind a 1.6-mm-thick stainless-steel aperture plate which itself was mounted vertically inside a light-tight stainless-steel and ceramic box.

In the aperture plate were drilled three 1-mm-diam holes arranged as shown in Fig. 3. Between aperture holes Nos. 1 and 2 and the scintillator was a 3-μm-thick aluminum foil which blocked plasma light and low-energy plasma particles, but passed the 1-MeV triton and 3-MeV protons from the D/D reaction. Between aperture No. 3 and the scintillator was a 21-μm-thick aluminum foil which stopped the 1-MeV tritons but passed the 3-MeV protons. The No. 4 channel was simply a spot on the scintillator behind the 1.6-mm-thick aperture plate, which stopped all particles and most x rays, but passed neutrons and gammas.

The idea was to measure tritons (with an estimated ≈30% contribution due to 3-MeV protons, as described below) in channels Nos. 1 and 2, to check the 3-MeV proton signal in channel No. 3, and to look for backgrounds due to neutrons, gammas, or hard x rays in channel No. 4. I will call channels Nos. 1 and 2 the "triton" channels with quotation marks, since the signals contain components due to 3-MeV protons and to backgrounds. Note that the two "triton" channels are separated vertically by about 2 mm, which turns out to provide a useful check of their triton detection capability (see below).

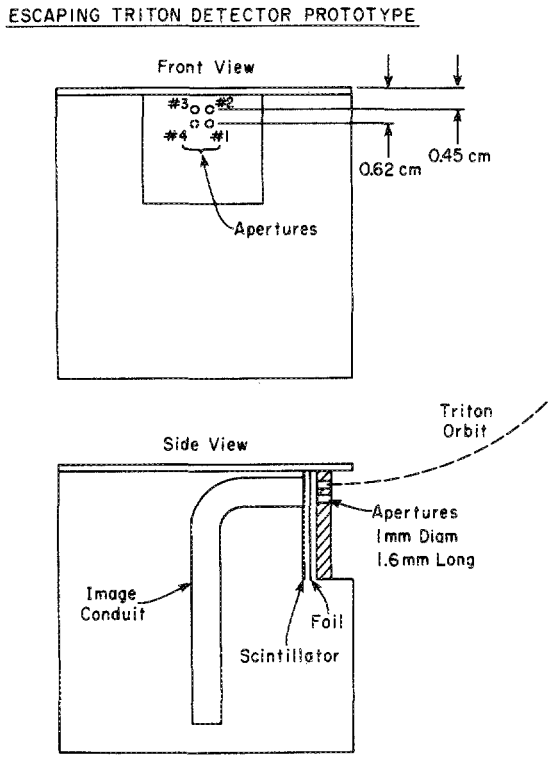

FIG. 3. Aperture design of the four-channel triton probe. Channels Nos. 1 and 2 were for measuring tritons (3-μm foil), channel No. 3 was for 3-MeV protons (21-μm foil), and channel No. 4 was for backgrounds (1600-μm "foil"). The vertical separation between the top of the box and channels Nos. 1 and 2 was important in determining whether the escaping triton orbits could enter the apertures.

The light (400–500 nm) from these four spots on the scintillator passed through the thin glass substrate and was proximity focused onto a coherent glass image conduit (0.25 in. diameter with 100-μm fibers), which brought the image of the four channels to a small lens, as shown in Fig. 2. There it was imaged with × 1 magnification across a vacuum window onto four separate 1-mm-diam quartz fibers, one for each aperture channel. These fibers passed through a secondary vacuum seal and then ran about 10 m to detectors in the TFTR basement. The optical system was aligned and focused before installation by first removing the scintillator and foils from the detector end, and then examining at the exposed end of the image conduit the focal spots of a light source sent from the other (detector) end of the quartz fibers.

Care was taken to mount the glass components securely to prevent breakage due to vessel vibrations during plasma disruptions. The glass pieces and also the stainless-steel detector box as a whole were undamaged after 4 months of operation in TFTR; however, there was a slight radiation-induced darkening of the glass image conduit (which could be avoided in the future by using polyimide-jacketed quartz fibers). The top and sides of the detector box were coated with a thin layer of carbon due to vapor deposition; however, the aperture foils were not perceptibly coated or damaged during this period. The probe temperature as monitored by an internal thermocouple (see Fig. 2) was always < 50 °C for the present probe position.

II. EXPECTED TRITON SIGNALS

This detector was installed so that the top of the box was positioned 9 cm below local poloidal limiters, which were surface pumping panels (SPP) located on either side toroidally from the box. The apertures were facing outward along the major radius of the torus. This location and orientation imposed a strong geometrical constraint on the triton orbits, which, along with the plasma conditions, determined the expected triton signals.

This constraint is described in Fig. 4, which shows the location of the triton probe with respect to the TFTR vacuum vessel, the local poloidal limiters, and a typical plasma (major raidus $R = 265$ cm, minor radius $a = 80$ cm, $I = 0.8$ MA, $B = 28$ kG). Figure 4(a) also shows the trajectory of a 1-MeV triton orbit which enters one of the apertures at a pitch angle of 87.4° with respect to the plasma current direction (note that the orbit is actually calculated "backwards in time" from the aperture back into the plasma, as described in Ref. 2). This orbit moves both vertically into the plasma and also toroidally, such that it just barely misses the local SSP, which is about 20 cm away toroidally and 9 cm vertically above the probe. Similarly, the orbit in Fig. 4(b) which enters the aperture at a pitch angle of 84.5° just barely misses the local limiter about 10 cm away toroidally (on the other side) and 9 cm vertically above the probe.

Thus, in order to reach this detector's apertures without being intercepted by the local obstacles on either side toroi-

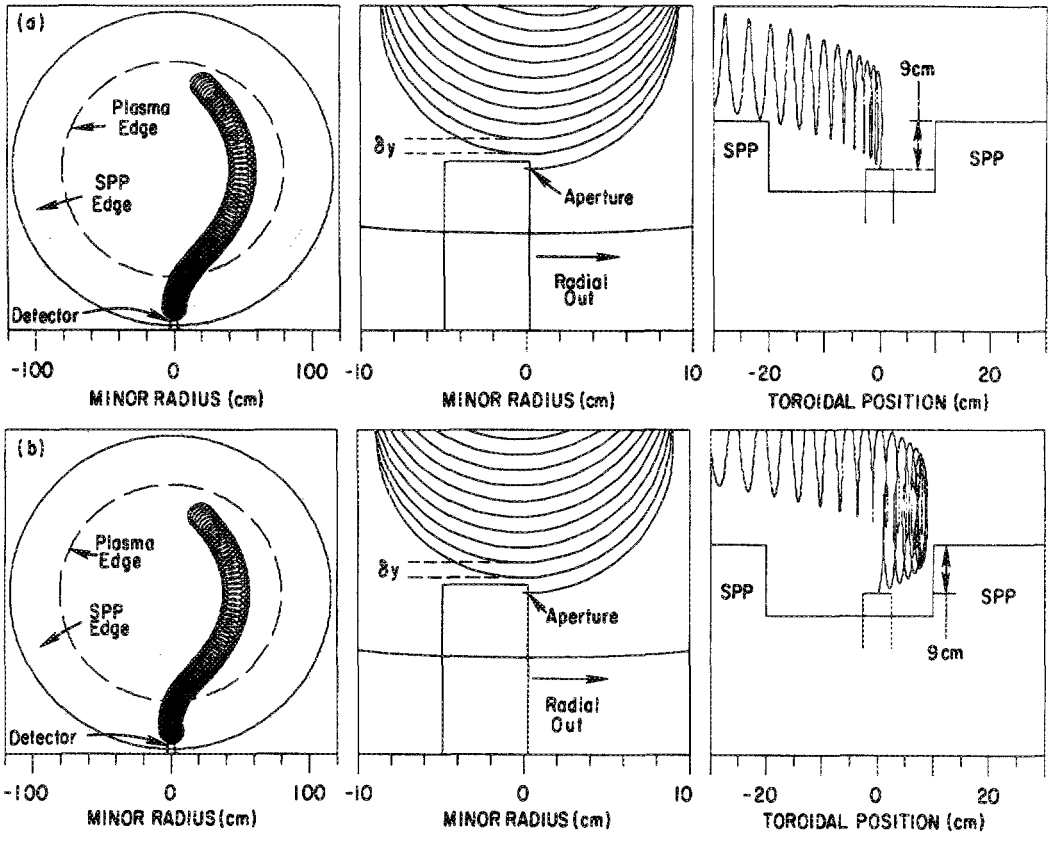

FIG. 4. Orbits of 1-MeV tritons which can enter the detector apertures. Since the detector is located 9 cm below local obstacles (SSP), there is only a narrow range of pitch angle over which the escaping orbit can reach the detector. This range is defined by the orbits in (a) and (b) where the pitch angle is 84.7° and 84.5°, respectively (with respect to the toroidal field).

dally, a triton orbit had to be moving nearly vertically downward just above the detector, i.e., with a pitch angle in the range 84.5°–87.4° as measured at the detector. The tritons which enter the detector are, therefore, expected to originate from somewhere along the trajectories or "sightlines," as shown in Fig. 4.

In addition to this pitch angle constraint, the last orbit before entering the aperture orbit must miss the top of the detector box itself, as shown in Fig. 4. Since for pitch angles of about 90° this last orbit is located within the toroidal extent of the 2 in. × 2 in. detector box, the last orbit must drop vertically by at least the distance between the box top and the aperture hole in order to enter the aperture hole. It can easily be shown[2] that the vertical drop per orbit, δy_{orbit} for particles with nearly 90° pitch angle is defined entirely by the triton's *toroidal* gyroradius $\rho = v_{\text{triton}}/eB/mc$) and the major radius of the detector R; thus a required condition for tritons to enter an aperture which is $\delta y_{\text{aperture}}$ below the top of the detector is

$$\delta y_{\text{orbit}} = \pi\rho^2/R > \delta y_{\text{aperture}}. \quad (1)$$

Thus, for a given detector position, triton energy, and aperture location, the orbit is expected to enter the aperture only *below* a certain toroidal field (i.e., only above a certain gyroradius). For this detector's position $R = 265$ cm at a triton energy of 1 MeV, this condition on B for detecting tritons in a particular aperture is

$$B < 27 \text{ kG } (\delta y_{\text{aperture}}/1 \text{ cm})^{-0.5}. \quad (2)$$

Thus, for channel No. 1 with $\delta y = 0.62$ cm, the triton flux should be extinguished for $B > 34$ kG, while for channel No. 2 with $\delta y = 0.45$ cm, the triton flux should be extinguished for $B > 40$ kG. This effect was observed in the data, as described in Secs. IV and V.

Assuming that these two geometrical constraints on triton orbits entering the detector are satisfied, the orbit sightlines can be calculated back into the plasma, as shown, in Fig. 4. For the unobstructed range of pitch angles at the detector, the orbit code calculated a detection efficiency ϵ, defined[1,2] as the ratio of the number of expected tritons (for a given detector area and aperture solid angle) to the total number of tritons (i.e., 2.5-MeV neutrons) created in the plasma. The calculated efficiencies for this detector are shown as a function of plasma current in Fig. 5.

The two main determinants of the expected triton flux as shown in Fig. 5 are the plasma current and the neutron source profile. As the plasma current is increased above 0.8 MA (the current used in Fig. 4), the triton orbits tend to follow more closely the magnetic flux surface which goes through the detector, so that the sightlines become weighted more toward the outer plasma edge than those in Fig. 4. Since the neutron (and triton) source profile is peaked at the plasma center, the resulting detection efficiency ϵ (averaged over the sightline) decreases with plasma current. Similarly, at fixed plasma current, ϵ increases as the shape of the neutron source profile {parameterized as $S_n(r) \propto [1 - r/a)^2]^{IS}$} becomes more flat, since these sightlines go through the region $r/a > 0.5$. Note that for Fig. 5 the actual detector location, aperture, and local poloidal limiter boundaries were used to compute ϵ; the resulting detection efficiency is typically $\approx 10^{-9}$. Thus, for a typical neutron (triton) source rate of $S_n \approx 10^{15}$ n/s the expected triton flux through the 1-mm-diam aperture is $S_t \approx 10^6$ tritons/s.

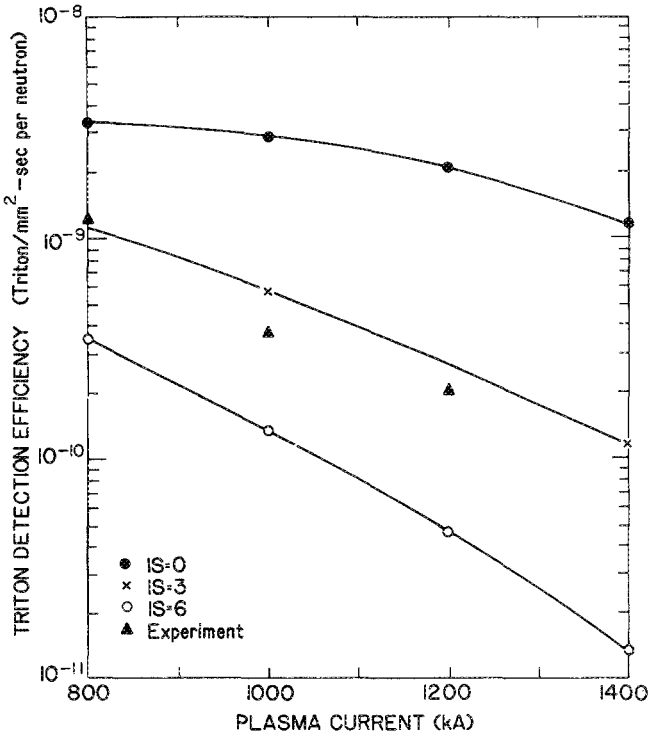

FIG. 5. Theoretically calculated efficiency curves for expected triton flux with the present detector position, aperture orientation, and local obstacles. The curves for various neutron (i.e., triton) source profiles are labelled by *IS* (parabolic exponent). The experimental results for three plasma currents are also shown.

Note that although the curves for Fig. 5 were drawn assuming a current profile shape of $J(r) \propto [1 - (r/a)^2]^{IC}$, where $IC = 3$, the resulting efficiencies vary by only about 30% over the plausible range of current profile exponents $IC = 2$–4.

III. SIGNAL HANDLING AND CALIBRATION

Two different methods of handling the optical output of this system were tried: (a) pulse-height analysis using photomultiplier tubes and (b) flux monitoring using either photomultiplier tubes or a video camera. The potential advantages of the pulse mode are that some energy resolution and some pulse-height discrimination against backgrounds are possible. The advantages of the flux mode are its wide dynamic range and relative simplicity. Although the initial design was based on method (a), it turned out that the method (b) was much more useful in practice and better suited to future uses of this detector.

A. Pulse-height system

An outline of the signal path is shown in Fig. 1. For each of the four channels, the light signal was sent to the shielded basement through a 1-mm quartz fiber. For the pulse system this fiber was proximity coupled to an RCA 6342A PM tube, the output of which went successively to an ORTEC 113 preamplifier, an ORTEC 471 spectroscopy amplifier, one or more ORTEC 550 single-channel analyzers (SCA), and to the TFTR computer system for recording pulse-height spectra and SCA counts versus time.

The response of the two 1-MeV "triton" channels Nos. 1 and 2 was bench tested and calibrated using a 241 Am alpha source of energy 4.5 MeV and count rate $\approx 3 \times 10^3$ alphas/s, as described previously.[10] A rather broad pulse-height spectrum was observed, due to the multicrystalline nature of ZnS and to the inefficient optical coupling between the scintillator and detector. During plasma shots an LED test signal was added into the PM tube to monitor possible gain shifts and pileup effects.

The main problem encountered using this type of signal handling in TFTR was pulse pileup due to an excessive triton count rate. The symptom of pileup was a severe distortion of the pulse-height spectrum (including the LED test pulses) with increased neutron source strength, and an associated SCA count rate of $> 10^6$ counts/s. This count rate was simply too high for this pulse system, even when the amplifier pulse width was reduced to ≈ 2-μs FWHM (the minimum consistent with the decay time of the scintillator). The count rate could in principle be reduced via the aperture area, but in practice could not be changed after the initial installation on TFTR.

There was also a persistent background problem which turned out to be due to soft x rays from the plasma. Although this background accounted for typically only 10%–15% of the light output of the detector (see Sec. IV), the x-ray pulses (with keV-level pulse heights) formed a slowly varying quasi-dc level which was not handled well by the standard pulse system, often producing base-line shifts comparable to the pulse-height range for tritons (even using the base-line restoration and bipolar output of the 471 amplifier).

These problems precluded the use of pulse counting for reliable triton detection in TFTR. Although both of these problems might have been solved with further design iterations, in the long run the pulse mode is undesirable because (a) the broad pulse-height spectra of multicrystalline ZnS makes energy resolution intrinsically difficult, (b) the expected count rate for D/T alphas of about 100 times that for D/D tritons would require that the aperture system be irreversibly changed between D/D and D/T, (c) pulse counting systems in general have a relatively small dynamic range, which restricts their ability to detect possible "bursts" of escaping particles, and (d) the high cost of discrete pulse counting channels would severely limit the multichannel imaging capability of ZnS. Therefore, the flux mode was used for all results described in this paper.

B. Photomultiplier flux system

The four-channel photomultiplier system was converted to a dc-coupled flux (i.e., current) mode. The PM outputs were buffered by a standard voltage follower (10-kHz bandwidth), amplified by an ORTEC 535 quad fast amp, and digitized by the TFTR computer system at typically 1 kHz. This flux mode system worked well for high-count-rate operation ($> 10^5$ counts/s) with typically $< 10\%$ rms fluctuations in the detected signal.

This system had the advantages of good time resolution and immediate archiving of the data onto the TFTR computer. The minor disadvantages were a slightly increased

neutron background (due to the large-area PM tubes compared to the small-area camera) and the need to cross calibrate the PM tube sensitivities. The major disadvantage for future applications is cost per channel, which matches that of the camera system at about 20 channels, thus preventing the use of individual channels for two-dimensional imaging applications.

C. Video camera flux system

The light flux from the scintillator was also measured by proximity coupling the four quartz fibers to the photocathode of a gated, intensified video camera (Xybion ISG-01). The sensitivity of this detection system was set through the gating interval of the internal microchannel plate (typically 100 μs). The camera's video output was recorded onto standard videotape in the "field" mode, i.e., with 16 ms between exposures. A constant light source was also recorded to check for possible gain changes caused by the internal automatic gain control. No such gain changes were present for the data discussed in this paper.

The recorded images were digitized by a PC-based image-processing system. The average intensity within the 1-mm-diam fiber images were found for each fiber versus time. The number of pixels within a fiber image was ≈ 1000, the typical pixel intensity level was 50 out of 256 maximum (i.e., far from saturation), and the background (off-fiber) level was typically < 1.

This system was quite easy to implement and reliable, although the data-processing scheme was too slow to digitize more than a few shots. The limited dynamic range of the videotape (≈ 100) was adequate for present use and could be improved substantially by computer control of the gating intervals (e.g., reducing the exposure time during times of high triton flux). The great advantage of this system is that it is capable of handling a large number of channels in parallel. Its main disadvantage is the relatively poor time resolution compared to the PM detector system.

D. Post-calibration

As mentioned previously, the initial calibration of the detector was made in the pulse-height analysis mode and not the flux mode. After the 4-month TFTR run, the detector was removed and post-calibrated in both modes.

The post-run pulse mode calibration of the 1-MeV "triton" channels Nos. 1 and 2 with the ^{241}Am source showed the same pulse-height spectrum and count rate for each channel as previous to the run.[10] However, this source was too weak to use for the flux mode calibration, and so a relatively strong ($\approx$1-mCi) ^{244}Cm alpha source was used instead.

The ^{244}Cm source strength was measured with a standard ORTEC silicon surface barrier detector using a mock-up of the aperture geometry ($\approx 3\times 10^4$ counts/s at $\approx$1-cm source-aperture spacing). This source's energy spectrum was measured to be approximately flat up to the maximum alpha energy of 5.8 MeV. Thus the absolute alpha energy flux for this source was known, at least within about $\pm$ 25% uncertainty. The calibration procedure consisted in using this same source-detector geometry to find the dc signal levels using the PM tube and video camera detection modes for each of the four detector channels.

The relative signal levels obtained using this alpha source calibration for the two "triton" channels No. 1/No. 2 was found to be 4.4 $\pm$ 1:1 (for both flux detection systems). This difference in sensitivity was found (after disassembly) to be due to an imperfect alignment between the 1-mm-diam scintillator spots and the 1-mm-diam optical fibers, which caused a different optical efficiency for the two channels. Since this alignment was set during the initial calibration and was unchanged through the run, it was easy to correct for in the final analysis.

As expected, the ^{241}Am alpha signals in the thick-foil 'proton" and "neutron/gamma" channels Nos. 3 and 4 were not detectable (i.e., $< 1\%$ that in channel No. 2). However, the same initial alignment also created two non-negligible ($> 1\%$) optical cross-talk paths, namely, $\approx 20\%$ of the signal into aperture No. 2 appeared in channel No. 1, and $\approx 20\%$ of the signal into aperture No. 3 appeared in channel No. 4.

The absolute triton flux sensitivities of channels Nos. 1 and 2 were then estimated from the alpha flux by assuming that the scintillator light output was proportional to the total energy loss of fast particles within the thickness of the scintillator. A 1.0-MeV triton after passing through a 3-μm aluminum foil has an energy of $\approx$0.75 MeV, and a typical 3-MeV alpha particle emitted from the ^{244}Cm source after passing through the same foil has an energy of $\approx$2.3 MeV. Since the ranges of these particles are comparable to the average thickness of the scintillator grains ($\approx 10\,\mu$m), I will assume that the relative response of this detector for 1.0-MeV tritons is $\frac{1}{3}$ that for the ^{244}Cm alphas. Obviously, this estimate is uncertain by at least a factor of 2 in the absence of a 1.0-MeV triton calibration source.

The expected sensitivity to 3-MeV protons was estimated similarly. Thus a 3-MeV proton after passing through a 3-μm foil should produce $\approx 30\%$ the scintillator light in ZnS of a 1.0-MeV triton passing through the same foil (since the proton's range in the scintillator is $\gg 10\,\mu$m), and a 3-MeV proton after passing through a 21-μm foil (channel No. 3) should produce $\approx 40\%$ the scintillator light output in ZnS of a 1.0-MeV triton passing through a 3-μm foil.

An attempt was also made to check this detector's response to soft x rays and neutrons. A KEVEX soft x-ray generator was used to illuminate the detectors uniformly with bremsstrahlung radiation (25–45 keV beam energy). It was found that the ratio of soft x-ray signals in channel No. 1/No. 3 was 5.6 $\pm$ 1/1, and that the difference in foil thickness between these channels could account for only a ratio of 1.4. Thus the optical coupling efficiency of channel No. 3 was $\approx \frac{1}{4}$ that of channel No. 1, again due to the imperfect initial alignment (no proton source was available to check directly the response of channel No. 3). Also, the soft x-ray test revealed the cross talk of channel No. 3 into channel No. 4, as mentioned above (no soft x rays could directly pass the 1.6-mm "foil" of channel No. 4).

No 2.5-MeV neutron calibration source was available which could make a measurable signal in this detector; how-

ever, an optical cross calibration of the efficiency of channel No. 4 was made after disassembly. The expected sensitivity of the scintillator to neutrons, gammas, and soft x rays is discussed in Appendix B.

In summary, the post-calibration produced an estimate of the absolute triton detection sensitivity of channels Nos. 1 and 2 (with an uncertainty of at least a factor of 2) and of the relative optical efficiencies of channels Nos. 1–4 (with an uncertainty less than a factor of 2). Two optical cross-talk paths associated with imperfect optical coupling were also found. Given these difficulties in cross calibration, channels Nos. 3 and 4 were not immediately used for background subtraction; rather, the variation of triton flux with the toroidal field B in channels Nos. 1 and 2 was used as the primary check of triton detection, as described below.

IV. EXAMPLE OF TRITON DETECTION IN TFTR

A. Triton-channel signals

In Fig. 6 is an example of the measured flux versus time in the "triton" channels Nos. 1 and 2 for a typical TFTR neutral-beam-heated discharge. For this case the video camera was used to monitor the signal at a sampling speed of 60 Hz. The toroidal field was $B = 28$ kG (at 0.8 MA plasma current), so that the triton orbits should have been able to reach both channels equally well [see Eq. (2)]. Figure 6 shows that the time dependences of both channels Nos. 1 and 2 were similar to each other and to the neutron source rate, as expected from a simple prompt-loss triton confinement model.[11]

In Fig. 7 is a comparison of these "triton" signals for three TFTR shots with $B = 28$, 39, and 47 kG, all at 0.8 MA plasma current. Since the neutron fluxes were identical to within $\pm$ 5% for these three shots (and other plasma conditions were very similar), the difference between these signals is almost certainly due to the geometrical triton orbit constraint discussed in Sec. II. That constraint predicts that the triton flux in channels Nos. 1 and 2 should be extinguished above 34 and 40 kG, respectively.

The results of Fig. 7 agree quite well, but not completely, with this expectation. In channel No. 1 the flux decreased by

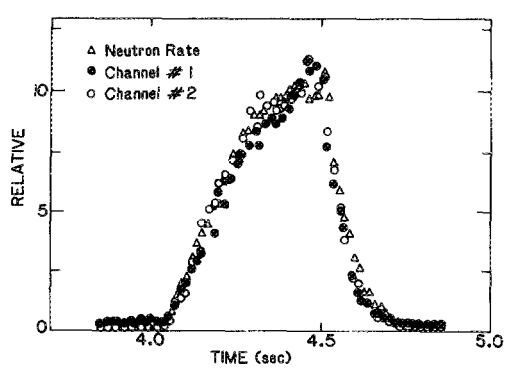

FIG. 6. Examples from a typical TFTR shot of measured "triton" flux in channels Nos. 1 and 2 vs neutron source strength. The time dependence of the "triton" flux is approximately the same in Nos. 1 and 2, as expected at $B = 28$ kG, and roughly the same as the neutron (triton) source rate, also as expected. Note that the magnitudes of channels Nos. 1 and 2 are normalized to appear approximately equal.

about a factor of 4 between 28 and 39 kG, and by about a factor of 15 between 28 and 47 kG. The partial extinction of the signal at 39 kG is most likely due to several small effects which broaden the expected extinction threshold (see Appendix C), but complete extinction should have been obtained at 47 kG, instead of the 6% residual signal as shown. In channel No. 2 the signal at 28 kG was about the same as that at 39 kG as expected, but again there was a residual signal of about 12% at 47 kG where complete extinction was expected. These results suggest that there was a nontriton background superimposed on these "triton" signals.

The expected absolute flux of tritons into channels Nos. 1 and 2 was calculated with the triton orbit code using the plasma current profile as estimated from the measured plasma temperature profile (i.e., $IS = 3$ in the notation of Sec. II), and the aperture sizes, orientation, and approximations of the local obstacles present in this experiment. The main uncertainty in this calculation was from the assumed neutron source profile, which could potentially vary from $IS = 6$ (in the notation of Sec. II) to $IS \approx 0$–3. The former is the value determined from a calculation based on classical beam-ion penetration without beam-ion diffusion, while the latter might be obtained if the beam particles ionized or diffused anomalously. This range of assumptions produces a $\times 10$ variation in the expected flux at the detector for 800 kA, as shown in Fig. 5. For the usual assumption of $IS = 6$, the calculated flux for $I = 0.8$ MA for a detector area 0.75 mm^2 and a neutron flux of 1.8×10^{15} neutrons/s is $\approx 7 \times 10^5$ tritons/s. The same flux is expected for both channels Nos. 1 and 2 at 28 kG.

The measured triton flux based on the post-calibration described in Sec. III D was $\approx 2 \times 10^6$ tritons/s for both channels Nos. 1 and 2 at the peak neutron flux of 1.8×10^{15} neutrons/s for the 28-kG shot of Figs. 6 and 7. This estimate includes a 30% correction for the expected 3-MeV proton contribution to the signals in channels Nos. 1 and 2, but not the $\approx$30% correction for the soft x-ray and neutron backgrounds (see below), which would then reduce the measured flux to $\approx 1.5 \times 10^6$ tritons/s, i.e., about twice the calculated flux. Thus the measured signal tentatively attributed to tritons in channels Nos. 1 and 2 is consistent with the expected signal from tritons based on the simplest theoretical model, at least within the $\times 2$ uncertainties of both the neutron source profile shape and the detector calibration.

The conclusion from this example is that the signals observed in the two "triton" channels were roughly consistent with the expected triton signals with respect to their time dependence, magnetic field dependence, and absolute magnitude. The nontriton component of these "triton" channel signals was from the backgrounds described below.

B. Background signals

In Fig. 8 is an example of the signal from channel No. 1 for a case when the plasma current is very high (2.2 MA) and the expected triton flux is very low ($\approx 10^{13}$ n/s). The signal is monitored using a photomultiplier in this case. It is evident that channel No. 1 responds to something other than tritons, since it shows a significant signal level before the rise in neutron (triton) creation due to neutral beam injection.

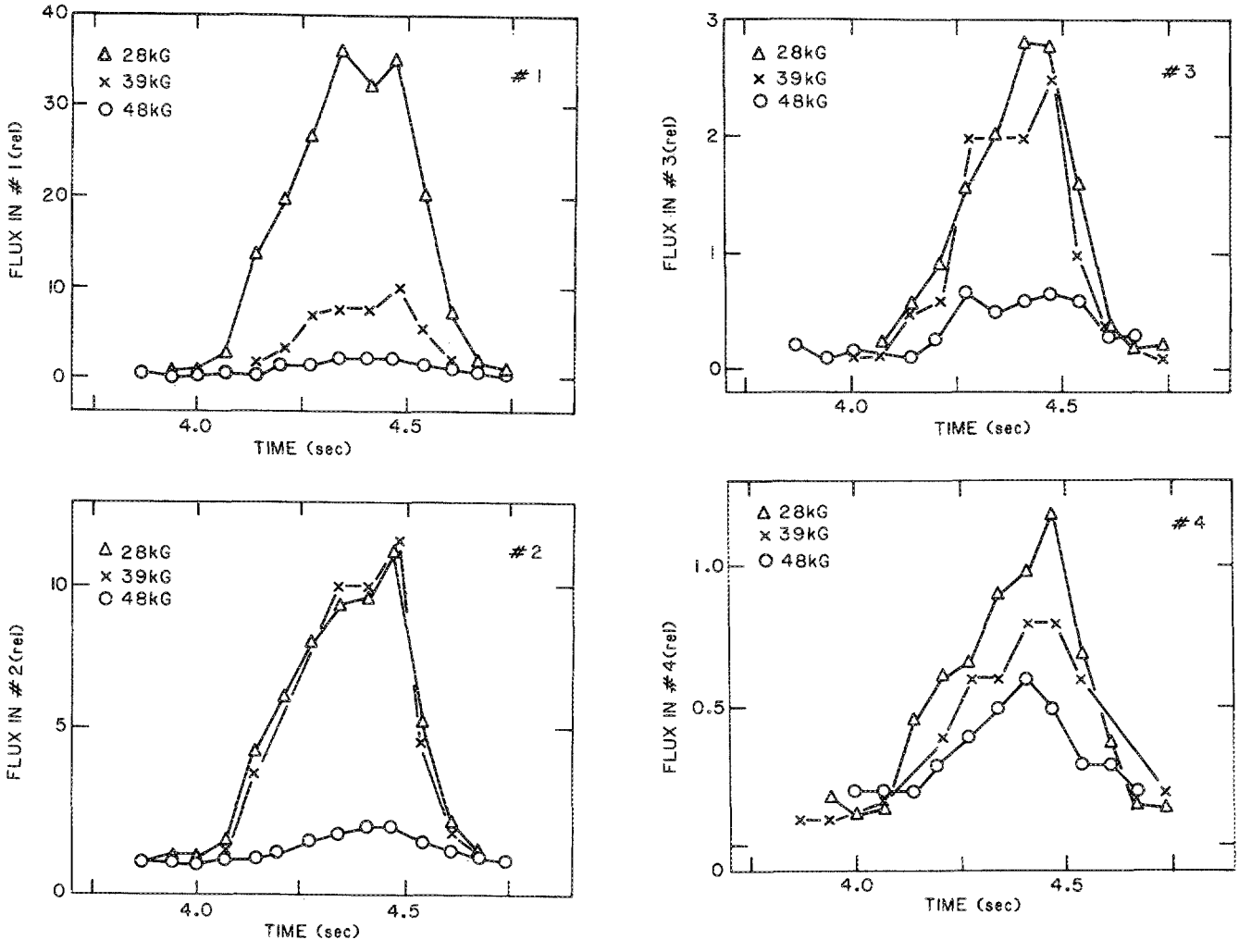

FIG. 7. Examples of the effect of toroidal field B on the flux in channels Nos. 1–4. Increasing B reduced the signals in channels Nos. 1 and 2 approximately as expected from Eq. (2). The residual signals at $B = 48$ kG are mainly due to backgrounds. In this figure the fluxes are uncorrected for the relative channel-to-channel optical efficiency.

The time dependence of channel No. 1, in fact, looks very similar to that of the soft x-ray emission as monitored by a central chord of the x-ray diode array. Note that the soft x-ray flux at 2.2 MA is ≈ 10 times larger than at 0.8 MA due to the higher plasma temperature and density.

This background in the "triton" channels associated with soft x rays is most likely due to x-ray reflection from the vessel walls into the aperture (which itself does not view the plasma). The expected background is estimated in Appendix B and evaluated *in situ* in Sec. V.

Another source of background was made clear when the probe was retracted from the vessel and isolated from the plasma behind a closed vacuum valve, in which case a signal in all channels with a time dependence of the neutron flux was observed. This background was caused by either neutrons or gammas (from neutron capture reactions) interacting with the scintillator itself, the fiber optics, or the detector. This background is discussed in Appendix B and evaluated *in situ* in Sec. V.

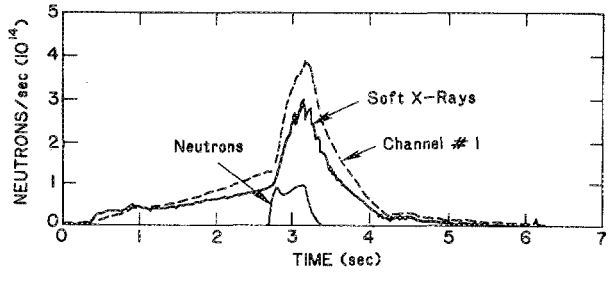

FIG. 8. Example of the soft x-ray background as seen in channel No. 1. This TFTR shot had a high level of soft x rays before the neutral beams are turned on at 2.8 s, during which time the triton creation rate was negligible.

V. BACKGROUND-CORRECTED TRITON SIGNALS

Here the background contributions in the "triton" channels are evaluated *in situ* and the corrected signals are plotted versus B for a larger set of TFTR plasmas. The results show good agreement with the expected B dependence of the triton signal discussed in Sec. III, indicating that these detectors are indeed measuring tritons.

The soft x-ray correction was made by examining the observed signals during high-B, high-current non-beam-heated plasmas when the triton source was negligible

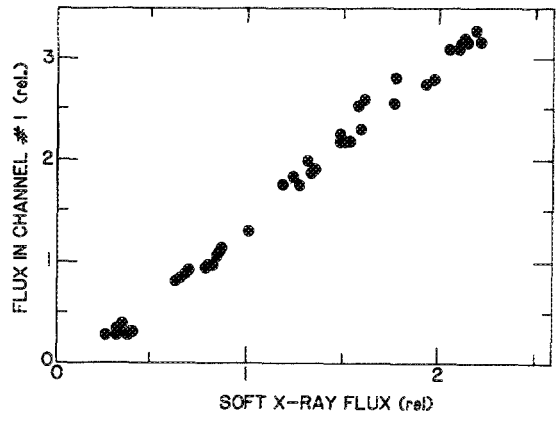

FIG. 9. Correlation between the background signal in channel No. 1 and the soft x-ray flux. These data were taken from 50 high-current shots during which soft x-ray flux was large and the triton source rate was negligible. The maximum level of soft x rays during a low-current shot (as in Fig. 6) was about 0.45 (in these units).

($\approx 10^{-2}$ that during typical neutral beam injection). The observed signals were closely proportional to the soft x-ray flux, as shown for channel No. 1 in Fig. 8 and summarized in a data base for channel No. 1 from about 50 shots in Fig. 9. Note that the approximately constant position of the soft x-ray source and the diffuse nature of the wall reflection make this calibration factor approximately constant for all these experiments.

The proportionality constant between the observed soft x-ray background and the soft x-ray level was used during low-current beam-heated shots to correct the signals for the soft x-ray background. This resulted in a "triton" signal correction of $\approx 10\%$–15% in channels Nos. 1–3 for low-current beam-heated shots like in Figs. 6 and 7. The soft x-ray background in channel No. 4 was consistent with the measured cross talk between channel Nos. 3 and 4 (i.e., consistent with the assumption that the soft x-ray background entered the detectors through the apertures).

The neutron/gamma correction was made by observing the signals during beam-heated discharges during which the probe was retracted by about 50 cm and isolated behind a vacuum valve. These observed background signals were linearly proportional to the neutron flux and approximately the same in all four channels (after cross calibration), as expected. The proportionality constant between observed neutron background and measured neutron flux was used to correct for this background. This correction was $\approx 15\%$–20% for channel No. 1 and 30% for channel No. 3 for typical low-B, low-current discharges. Note that there is an uncertainty of up to $\times 2$ in this correction due to the difference in neutron/gamma flux between the retracted versus the in-vessel probe positions.

These two correction factors were applied to the signals from "triton" channels Nos. 1 and 2 for a series of about 25 0.8-MA shots where B was varied between 21 and 48 kG, with results as shown in Fig. 10. The corrected data show good agreement with expected extinction of the triton signal above $B = 34$ and 40 kG, respectively. Note that the vertical axis here is "triton flux/neutron" to normalize for varying neutron rates in these shots. At low B, the triton flux in channels Nos. 1 and 2 is $\approx 2\times 10^6$ t/s at a neutron flux of 10^{15} n/s, or about 1×10^6 t/mm^2 s str at this $\approx 90°$ pitch angle and this neutron flux.

In particular, the reduction of the signal in channel No. 1 by a factor of about $\times 30$ between $B = 28$ and 48 kG im-

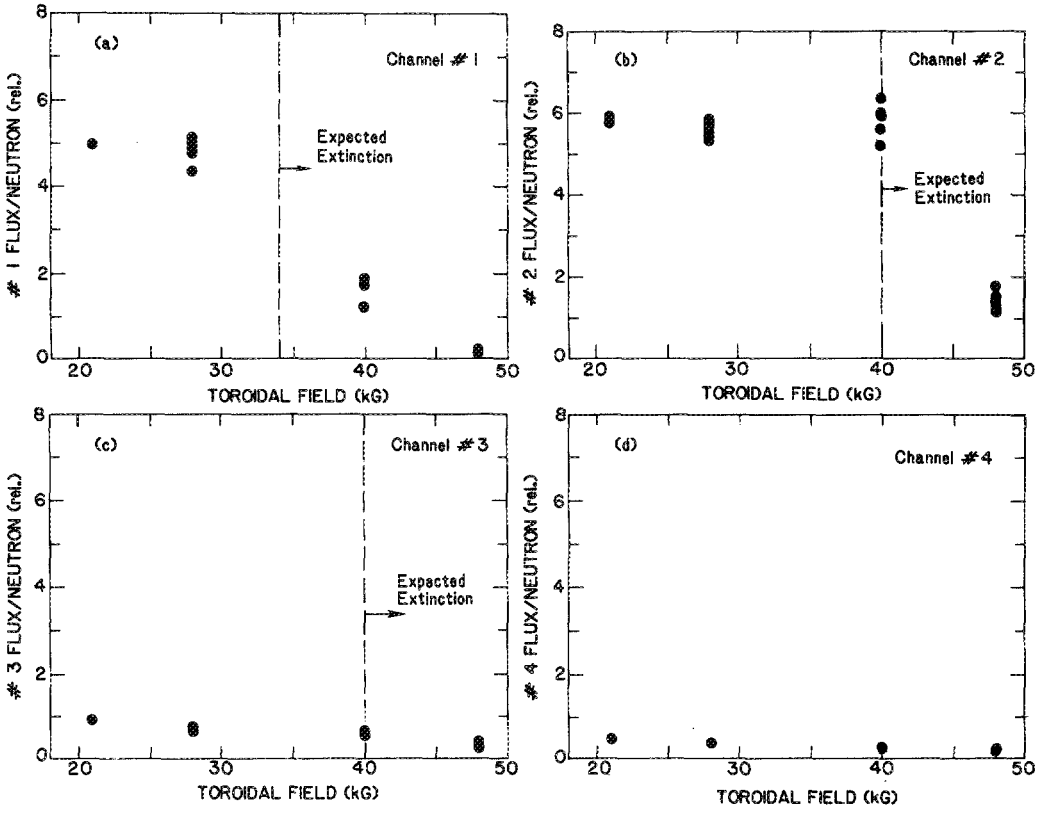

FIG. 10. Background-corrected flux in channels Nos. 1–4 vs B. The expected extinction of the triton flux in channel No. 1 above $B = 34$ kG and channel No. 2 above 40 kG is clearly seen in (a) and (b), indicating that these channels are successfully detecting tritons. The proton flux in channel No. 3 in (c) is also extinguished similarly to channel No. 2, as expected. The residual signal in the "background" channel No. 4 in (d) is due to cross talk from channel No. 3. Note that in this figure the four signals levels are corrected for the differing optical efficiencies, i.e., the signals in channels Nos. 1 and 2 at $B = 28$ kG are nearly equal at level of $\approx 10^6$ tritons/mm^2 s str. In each case there are two shots at 21 kG, seven shots at 28 kG, six shots at 39 kG, and eight shots at 48 kG.

plies that the over 95% of the background-corrected signal at 28 kG is due to tritons (plus 3-MeV protons which have identical orbits). Note that the signal levels in channels Nos. 1 and 2 at low B were equal to each other to within about 20% (after correction for the relative optical efficiency), as expected, and their absolute magnitude at 28 kG was roughly consistent with the expected flux (see Sec. IV).

The background-corrected signal from the "proton" channel No. 3 showed a B dependence similar to that of triton channel No. 2, as expected from its equivalent aperture location and the equivalent triton and proton orbits. The signal level was $\approx 10\%$ that of channel No. 2, somewhat lower than the expected $\approx 30\%$ signal for 3-MeV protons compared to 1-MeV tritons plus 3-MeV protons (probably due to the imprecise optical cross calibration). The background-corrected signal from the "neutron/gamma" channel No. 4 showed a small residual signal consistent with the optical cross talk between channels Nos. 3 and 4 measured in the post-calibration. Note that neither the soft x-ray background nor the neutron backgrounds varied with B when normalized in this way.

In conclusion, after the soft x-ray and neutron/gamma background corrections were applied to channels Nos. 1–3, their signals were consistent with the expected B dependence of 1-MeV tritons and 3-MeV protons. Since there is no other known reason why these signals should vary with B in this way, this is strong evidence for the triton (or proton) source of these signals.

VI. OTHER MEASUREMENTS

A. Plasma current dependence

A brief test of the plasma current dependence of the triton flux was made for 28-kG plasmas similar to those shown in Fig. 6. The results for $I = 1.0$ and 1.2 MA, as plotted in Fig. 5, show approximate agreement with the expected reduction in triton flux at higher I. In this case the measured triton flux/neutron was reduced by ≈ 6 at 1.2 MA compared to 0.8 MA, while the expected reduction was $\times 4$–7 (for neutron profile exponents $IS = 3$–6). Since the calculated neutron source had $IS \approx 7$ at 0.8 MA and $IS \approx 4$ at 1.2 MA, these results are consistent with expectations.

B. Alpha particle measurement

A brief test of alpha detection was made using deuterium beam injection into a ^{3}He plasma, where the dominant fusion reaction produces 3.7-MeV alpha particles and 15-MeV protons. The 3.7-MeV alpha particle has an orbit and foil transmission similar to that of the 1-MeV triton, and so should be detected in the "triton" channels Nos. 1 and 2 at low B.

At $B = 28$ kG the measured signal in channel No. 1 during D-^{3}He was $\approx 15\%$ of the measured signal during a similar D–D plasma (after the usual background subtractions). However, the measured neutron flux during the D-^{3}He shot was only $\approx 4\%$ (0.75×10^{14} n/s) of the neutron flux during the similar D-D shot. Therefore, most of the signal in channel No. 1 observed during D-^{3}He could be attributed to alphas (or to 15-MeV protons), and not to D-D tritons.

Although there was no direct measurement of the D-^{3}He reaction rate in this experiment, the results can be compared to the predicted reaction rate from the standard (time-independent) TFTR modeling code. Since the expected signal from a 3.5-MeV alpha is about $\times 3$ larger than for a 1-MeV triton, and the contribution of 15-MeV protons is expected to be about 1 MeV/proton (since the energy deposition is much less in the thin scintillator despite the $\times 5$ larger flux for these orbits), the inferred reaction rate of 3.7-MeV alphas is $\approx 5 \times 10^{13}$ α/s (based on comparison with a similar D-D shot). The calculated reaction rate was $\approx 1.2 \times 10^{14}$ α/s, with an uncertainty of at least a factor of 2. Therefore, the observed signals during D-^{3}He plasmas are consistent with the expected signals from alpha particles.

VII. DISCUSSION

This paper described the operation of a new type of scintillation detector for charged fusion products in tokamaks. The advantages of this detector are its simplicity, its relatively low neutron/gamma background sensitivity, its good time and space resolution, its optically coupled (low EMI) output, and its high neutron damage threshold (assuming the glass components are replaced with quartz). Its present disadvantages are its lack of energy resolution, its relatively low operating temperature range (< 100 °C), and its susceptibility to a wall-reflected soft x-ray background.

Potential improvements to this design can possibly circumvent these disadvantages through the use of a multichannel foil transmission measurement of particle energy and/or a higher-temperature scintillator. The soft x-ray background can be monitored with a particle-blind detector channel (≈ 100-μm aluminum) during D-D plasma operation, and should be negligible during D-T operation (when the alpha flux will be ≈ 100 times higher).

In its present configuration this type of detector would be most useful when positioned above the local obstacles instead of below them (as in this experiment), since then it would have an unobstructed view of pitch angles which correspond to particles coming from near the plasma center (at about 60° with respect to B). This should increase the triton flux by at least $\times 10$, according to the orbit code, without increasing the backgrounds. However, since most of the tritons will then approach the box with a toroidal as well as a vertical velocity component, the possibility of discriminating tritons from backgrounds on the basis of B will be lost. At that position the probe might also overheat and endanger its primary vacuum seal. These two potential difficulties can be avoided by reconfiguring the probe to avoid a direct line of sight between the wall x rays and the scintillator, and to image the scintillator at a vacuum interface far from the probe. An upgraded design along these lines is under development.[11] Such a design can also provide pitch angle resolution with a pinhole-slit aperture combination, similar to that used previously to measure alpha particles with a Cr-39 plastic track detector in PLT.[12]

ACKNOWLEDGMENTS

Thanks go to many people at TFTR who helped with this project, including T. Deverell, K. Hill, L. Johnson, P.

LaMarche, S. L. Liew, D. Manos, K. Owens, J. Strachan, and K. Young. This work was supported by the U.S. Department of Energy Contract No. DE-AC02-76-CH03073.

APPENDIX A: PROPERTIES OF ZnS SCINTILLATORS

ZnS has been used to detect alpha particles since Rutherford, as described in the standard references (Birks[13] and Knoll[14]). In the present experiment the scintillator screen was made from the standard blue ZnS(Ag) phosphor material (P11) with grain size 10.4 μm and average thickness 6 mg/cm^2 (i.e., about 1–2 grains thick). It was coated onto a glass microscope cover slide by Thomas Electronics (Wayne, NJ).

The efficiency of converting alpha particle energy into scintillation light for such ZnS(Ag) screens is $\approx$0.2–0.3,[13] so that typically $>10^5$ blue photons are created for each alpha particle. The ranges of 3.5-MeV alphas and 1.0-MeV tritons in ZnS are both $\approx$10–15 μm,[15] i.e., well matched to the scintillator thickness.

The spectral characteristics, sensitivities, and time constants of various phosphors are described in Ref. 16. ZnS(Ag) was chosen here mainly because of its high brightness, which is about $\times 2$ that of green ZnS(Cu) phosphor (P31) for our detectors. ZnS(Ag) also has a fast time constant ($<10\,\mu$s) and negligible long-persistence decay components. The light output should be linear with particle flux up to at least $\approx$1 particle ZnS grain-scintillation decay time, or 10^{11} particles/cm^2 s, which is large compared to triton fluxes $\approx 10^8$ cm^{-2} s in this experiment.

The main difficulty for future tokamak applications of ZnS(Ag) is the temperature dependence of its light emission. The light emission of the present screens due to ^{241}Am alpha particles was measured to be constant (to within $<10\%$) up to 100 °C, but fell rapidly ("quenched") above about 125 °C. Other phosphors such as P11 (green) and YtUEu (red) have higher quenching temperatures, but lower brightness. Note that ZnS(Ag) can be cycled to >400 °C without affecting its light emissivity below 100 °C.

Another potential difficulty of ZnS is that alpha bombardment eventually damages the phosphor by permanently reducing its light emission. A test made with a sample P11 screen showed $\approx\times 2$ reduction in light emission by alphas after exposure to $\approx 10^{13}$ α/cm^2 (from ^{241}Am), in rough agreement with the 30% reduction quoted in Birks.[13] The total triton flux during the present TFTR experiment was $\approx 10^{11}$ t/cm^2, i.e., negligible compared to the damage threshold. The expected flux for the same configuration for the TFTR D-T run would be $\approx 10^{12}$ α/cm^2, i.e., close to the damage limit.

Neutron damage to the ZnS phosphor will eventually occur due to (n,α) and (n,p) reaction products. For D-D the dominant reactions are ^{32}S$(n,\alpha)^{29}$Si and ^{32}S$(n,p)^{32}$P with a total cross section of $\approx$150 mb for 2.5-MeV neutrons. Thus the number of these reaction products created during this experiment was $\approx 4\times 10^3$/cm^2 on the scintillator, which is negligible compared to the damage threshold of ZnS. For D-T the total (n,α) and (n,p) cross section for ZnS is $\approx$500 mb, which for a total TFTR neutron flux of 10^{16} n/cm^2 gives $\approx 10^{11}$/cm^2, i.e., about 10^{-2} of the ZnS damage threshold. A test of 14-MeV neutron-induced damage to a sample ZnS screen was made with a neutron generator; after an exposure of $\approx 10^{12}$ n/cm^2 there was no detectable ($\ll 10\%$) change in the light emission with the ^{241}Am source. After exposure to $\approx 10^{13}$ n/cm^2 during the TFTR D-D run in 1986, the scintillator used in the present experiment also showed no measurable ($\ll 10\%$) damage.

APPENDIX B: BACKGROUNDS IN ZnS

The sensitivity of ZnS(Ag) to neutrons and gammas has been investigated previously,[13] since ZnS is often used for fast neutron detection. The counting efficiency of a 40-mg/cm^2 ZnS(Ag) screen for 2.5-MeV neutrons was measured to be $\approx 10^{-4}$, mainly due to the ^{32}S$(n,p)^{32}$P threshold reaction ($Q=0.93$), and $\approx 10^{-6}$ for 2.5-MeV gammas.[17] The efficiency for the present 6-mg/cm^2 screen is presumably lower. These can be compared to the counting efficiency of $\approx$1 for alpha particles.

A preliminary calculation of the expected neutron/gamma-induced backgrounds in ZnS(Ag) for alpha detectors in TFTR has been made by Liew of PPPL using the Monte Carlo MCNP and CYLTRANM codes.[18] He modeled the detector as a 10-μm-thick scintillator coated onto a quartz substrate (of varying thickness) exposed to typical neutron and gamma spectra at the wall of TFTR (both planar and isotropic for both D/D and D/T). Included in the code were relevant nuclear cross sections, elastic scattering of neutrons on Zn and S, Compton scattering of gammas, and magnetic field effects (on secondary electrons). Typical results were that for D/D (for an isotropic source with a 0.1-cm substrate at $B=5$ T) the expected energy deposition in the scintillator was $\approx$60 eV per incident neutron (with an n/γ flux ratio of 3.7), 85% of which was due to electrons entering the scintallator from Compton scattering of gammas in the substrate. For D/T the result was $\approx$270 eV per incident neutron (with an n/γ flux ratio of 1.4), 85% of which was due to Compton scattered electrons.

Application of this calculation to the present experiment implies that for a neutron source strength of 1.8×10^{15} n/s (Fig. 6) the neutron/gamma background in each channel should have been $\approx 2\times 10^8$ eV/s, or the equivalent of $\approx$200 tritons/s. The neutron/gamma background measured *in situ* was equivalent to $\approx$15% of the uncorrected triton signal at 28 kG, or $\approx 5\times 10^5$ tritons/s. Therefore, if this calculation is correct, then the background due to direct interaction with the scintillator was negligible in the present experiment. About half of this background was found to be due to direct interaction with the photomultiplier tube itself; presumably the rest was due to light produced by interaction of the neutrons or gammas with the fiber optics.

For future tokamak applications the neutron/gamma background can be monitored using a particle and soft x-ray blind detector channel like No. 4 in the present experiment. The (n,α) and (n,p) background components can be reduced somewhat by using other scintillators (e.g., ZnO); however, the Compton background seems very difficult to eliminate, since it can originate from any material within an electron gyroradius from the scintillator. Some other consid-

erations for "radiation-hardened" ZnS alpha detectors are discussed in Ref. 9.

The soft x-ray background in this experiment most likely came from the metal wall which is viewed by the apertures. Sesnic *et al.* previously measured a wall "reflectivity" of typically $\approx 10^{-4}$–10^{-3} in the 1–2-keV range in the PDX tokamak.[19] Given a typical soft x-ray flux to the wall of $\approx 10^{15}$ x rays/cm^2 s in the keV range for a TFTR plasma like in Fig. 6,[20] the estimated reflected x-ray flux into the apertures is equivalent to $\approx 10^6$–10^7 tritons/s into an aperture at the detector. This is roughly consistent with the observed soft x-ray background equivalent to $\approx 10^6$ tritons/s. (X-ray transmission through 3 m Al is $> 50\%$ in the ranges 1–1.5 keV, and that $> 10\%$ of the soft x-ray energy can be deposited in the scintillator.) Note that the direct soft x-ray flux from the plasma is much higher than this and would be dominant were it not for the stainless-steel box top, which attenuated the direct x–ray flux by $> 10^4$.

The hard x-ray flux due to runaway electrons was negligible compared to the gamma flux, except just after plasma disruptions when large bursts of scintillator emission correlated with signals in the NaI hard x–ray monitor were observed.

APPENDIX C: BROADENING OF THE EXTINCTION THRESHOLD

As mentioned in Sec. IV A, the expected extinction of tritons in detector channel No. 1 at $B > 34$ kG was not completely consistent with the observed $\approx 70\%$ extinction shown in Fig. 10, implying that some tritons reached the detector in apparent violation of Eq. (1). This is most likely due to the following effects which tend to broaden the expected threshold.

First, Doppler broadening of the triton birth energy will cause a spread in the expected gyroradius at the detector. For beam-target reactions (which dominate the triton creation rate) this energy spread is up to $\pm 25\%$, which results in a broadening of the critical B for extinction by about $\pm 12\%$ [see Eq. (2)]. Second, the finite aperture height of ± 0.05 cm results in a $\pm 10\%$ spread in $\delta y_{\text{aperture}}$, and so contributes another $\pm 5\%$ broadening of the B threshold. Together these two effects broaden the extinction threshold to about 34 ± 5 kG.

A third effect is due to uncertainty in the position of the local obstacle which is to the right of the detector in Fig. 4. The argument was made in Sec. II that the presence of this obstacle restricted the allowed range of pitch angles to those which must drop by δy_{orbit} in order to avoid hitting the box itself. However, Fig. 4 shows that this obstacle is very close to allowing orbits to enter the aperture whose last orbit was *not* within the toroidal extent of the detector itself. Therefore, this uncertainty can allow some tritons to be detected at fields above the critical B for intersection with the detector. For a maximum plausible position uncertainty of 3 cm, this would allow $\approx 10\%$ of the triton flux at 28 kG to appear in the detector at 47 kG.

Note that these orbits have negligibly different detection efficiency (per unit solid angle) over the accepted range of pitch angles and over the aperture area.

[1] R. E. Chrien and J. D. Strachan, Phys. Fluids **26**, 1953 (1983).
[2] W. W. Heidbrink and J. D. Strachan, Rev. Sci. Instrum. **56**, 501 (1985).
[3] J. D. Strachan, Rev. Sci. Instrum. **57**, 1771 (1986).
[4] H. -S. Bosch, U. Schumacher, and ASDEX team, in Proceedings of the 13th European Conference on Controlled Fusion and Plasma Heating, Schliersee, 1986, Vol. II, p. 124.
[5] G. Martin, O. N. Jarvis, J. Kallne, V. Merlo, G. Gadler, and P. van Belle, Phys. Scr. T **16**, 171 (1987).
[6] G. Dearnaley and A. B. Whitehead, Nucl. Instrum. Methods **12**, 205 (1961).
[7] S. Seiler and H. Hendel, Bull. Am. Phys. Soc. **23**, 701 (1978).
[8] T. Elevant, Royal Institute of Technology Report No. TRITA-PFU-84-4, 1984.
[9] G. H. Miley and H. Kislev, Phys. Scr. T **16**, 155 (1987).
[10] S. J. Zweben, Rev. Sci. Instrum. **57**, 1774 (1986).
[11] S. J. Zweben, Phys. Scri. T **16**, 119 (1987).
[12] T. J. Murphy and J. D. Strachan, Nucl. Fusion **25**, 383 (1985).
[13] J. B. Birks, *The Theory and Practice of Scintillation Counting* (Pergamon, New York, 1964).
[14] G. F. Knoll, *Radiation Detection and Measurement* (Wiley, New York, 1979).
[15] J. F. Ziegler, *The Stopping and Ranges of Ions in Matter* (Pergamon, New York, 1977); Vols. 3–5.
[16] "Optical Characteristics of Cathode Ray Tube Screens," TEPAC Publication No. 116 (EIA Tube Engineering Panel Advisory Council, 1980).
[17] P. G. Koontz, G. R. Keepin, and J. E. Ashley, Rev. Sci. Instrum. **26**, 352 (1955).
[18] S. L. Liew (private communication).
[19] S. Sesnic, F. H. Tenney, M. Bitter, K. W. Hill, and S. von Goeler, Rev. Sci. Instrum. **56**, 1160 (1986).
[20] K. Hill (private communication).